Fast Classification of Dust Particles from Shadows

Elio D. Di Claudio, Giovanni Jacovitti, Gianni Orlandi and Andrea Proietti
Department of Information Engineering, Electronics and Telecommunications (DIET), University of Rome "La Sapienza", Via Eudossiana 18, Rome, Italy

Keywords: Dust Monitoring, Object Classification, Contour Analysis.

Abstract: A fast and versatile method for classifying dust particles dispersed in the air is presented. The method uses images captured by a simple imaging system composed of a photographic sensor array and of an illuminating source. Such a device is exposed to free particulate deposition from the environment, and its accumulation is measured by observing the shadows of the particles the air casts onto the photographic sensor. Particles are detected and classified in order to measure their density and to analyse their composition. To this purpose, the contour paths of particle shadows are traced. Then, distinctive features of single particles, such as dimension and morphology, are extracted by looking at corresponding features of the sequence of local orientation changes of contours. Discrimination between dust and fibre particles is efficiently done using the varimax norm of these orientation changes. It is shown through field examples that such a technique is very well suited for quantitative and qualitative dust analysis in real environments.

1 INTRODUCTION

Detection and measurement of particulate air pollution is important in many applications, ranging from public protection from outdoor airborne particulate matter, to indoor air quality control, to environmental infection control in health-care facilities, to dust control into clean-rooms in semiconductor and biotechnology factories, to aerosol monitoring in museums and libraries, etc.

In particular, indoor air quality generally depends upon the outside environment, as demonstrated by the scientific community in the last years (Jones, 1999; Anderson et al., 2012; Delgado-Saborit et al., 2011; Frontczak and Wargocki, 2011). A critical element that decisively affects the indoors quality of the air is dust, especially due to the actual process of air circulation, much more limited than outside. Dust enters in indoor environments and persists there for a long time, increasing the chances of contamination and degradation due to environmental factors as light, temperature, and micro-organisms (Coronas et al., 2013).

The state of the art technologies for the monitoring of dust in indoor environments relies on the use of expensive equipment, often needing highly qualified staff and complex physical and chemical analysis, as spectroscopy, spectrometry, IR analysis, etc. Recently, other techniques have been developed, based on imaging systems. However, they often make use of very expensive microscopes and optical systems, as well as on chemical analysis or non-visible spectrum investigations (Chichinadze and Kvavadze, 2013; Ozga et al., 2013; Kyropoulou, 2013). These techniques are usually necessary to know the chemical composition of the particles, or when the environment is affected by very fine particles.

In many other cases, a less detailed knowledge of the dust, especially concerning the morphological information about the shape and the size of the dust particles, is sufficient. In particular, our application is mainly concerned with the estimation of the dust and fibre count in the airflow. Obtaining this information often requires the use of much less complex systems, with respect to the above-mentioned techniques. Pattern identification techniques using multiple features generally have high computational costs and the impact of each feature on the classification performance may remain unclear and undermine the generalization capabilities under different experiment settings.

A dust detection and analysis system based on image processing techniques was presented in a recent work (Proietti et al., 2014). It allows evaluating the dusting speed and some specific morphological information (i.e., shape and size of each dust deposition elements).

Di Claudio E., Jacovitti G., Orlandi G. and Proietti A..
Fast Classification of Dust Particles from Shadows.
DOI: 10.5220/0005218802410247
In *Proceedings of the International Conference on Pattern Recognition Applications and Methods* (ICPRAM-2015), pages 241-247
ISBN: 978-989-758-077-2

In this contribution, a very simple classification technique based on *particle contours* only is presented.

The first appealing aspect of this approach is that particle contours can be collected by using very simple imaging devices, such as the one illustrated in the forthcoming section.

The second advantage is that contours processing admits fast and accurate classification algorithms, permitting high repetition rate and low consumption operation. This performance is especially interesting if high spatial sampling over wide areas is required to relate for instance dust concentration to air flows, employing wireless sensor networks, where it demonstrated similar or better performance than some multi-feature approaches, as shown in Sect. 4.

2 SENSING APPARATUS

The acquisition stage is based on an USB Microsoft LifeCam HD-3000, which acquires 720p video images. The pixel size of its CMOS sensor is 3 μm^2, suited for capturing the finest particulate of interest in the present application. In fact, for our purpose, the camera was deprived of its lens, allowing the direct deposition of dust on the image sensor. The sensor was perpendicularly illuminated with a small white LED light source in order to create sharp shadows of particles in contact with the sensor. The sensor was tilted by 45° with respect to the floor to allow the deposit of dust, minimizing at the same time excessive accumulation.

A typical collection of particle shadows visible in an acquired image is shown in Figure 1.

Figure 1: The shadows of particles in a typical acquired image.

3 CONTOUR PROCESSING

The collecting time between cleaning operation is such that overlap of dust particles are rare events which do not statistically affect the significance of the measurements. This allows employing a fast detection and classification procedure described below.

Preliminarily, shadows are transformed in grayscale and hard limited to obtain binary images, where the inner part of any particle is black and the background is white[1].

The picture is then scanned by rows until the first non-singleton particle contour is encountered. The overall procedure is sequentially repeated on all shadows collected in the picture, by cancelling out extracted shadows and single spurious pixels.

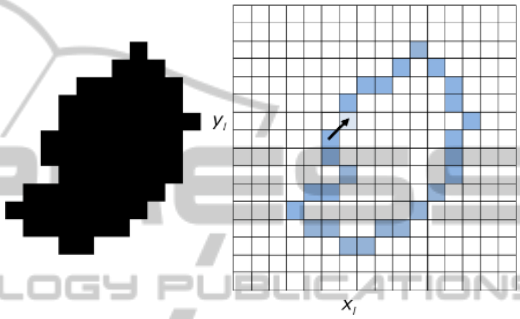

Figure 2: The particle shadow (left) and the one-step motion vector of the l-th boundary pixel (right).

Looking at the generic k-th particle depicted in Figure 2, its contour is first represented by the sequence of boundary pixels (the white ones adjacent to the black ones).

In order to characterize the topological relationship between the boundary pixels, these are listed in a cyclic matrix B_k containing their Cartesian coordinates x_l and y_l, ordered so that the distance of each pixel from the nearest one is at most one, both in horizontal and vertical direction, proceeding (without loss of generality) clockwise:

$$B_k = \begin{bmatrix} x_1 & y_1 \\ \cdots & \cdots \\ x_l & y_l \\ \cdots & \cdots \\ x_L & y_L \end{bmatrix}, \quad l = 1 \ldots L. \tag{1}$$

This matrix literally represents the k-th particle boundary, since it allows to graphically reconstruct it. Most important, it describes the dynamical behaviour of the contour, i.e., it accounts for the topological relationship between consecutive elements, just like con-

[1]Under the typical additive sensor noise (i.e., 2-10 standard deviation levels on a 255 grayscale image), the shadow extraction was nearly insensitive to noise, as shown in the experimental trials. For a 10 levels standard noise deviation, a DCT denoising stage (Foi et al., 2007) before the threshold operation allowed to regain the same performance as in the noiseless case.

secutive elements of a time series reflect the dynamical behaviour of the system generating it. Thus, in principle, a particle can be regarded as a system generating a double circular signal (the boundary) and we may look to the particle classification problem as a classical problem of system identification. To make this analogy more directly interpretable, let us consider the first backward row difference of this matrix, which defines a new cyclic matrix Δ_k as:

$$\Delta_k = \begin{bmatrix} \delta_{x1} & \delta_{y1} \\ \cdots & \cdots \\ \delta_{xl} & \delta_{yl} \\ \cdots & \cdots \\ \delta_{xL} & \delta_{yL} \end{bmatrix} , \tag{2}$$

where

$$\begin{aligned} \delta_{xl} &= x_{l \bmod L+1} - x_{(l-1) \bmod L+1} , \\ \delta_{yl} &= y_{l \bmod L+1} - y_{(l-1) \bmod L+1} , \end{aligned} \tag{3}$$

where "mod" indicates the modulus (positive remainder) operator. Hence, Δ_k entries δ_{xl} δ_{yl} can assume the eight possible pair values: $(1,0)$, $(0,1)$, $(-1,0)$, $(0,-1)$, $(1,1)$, $(1,-1)$, $(-1,1)$, $(-1,-1)$.

Using a well-known terminology employed in video coding, these pairs can be viewed as the motion vectors of a generic boundary pixel travelling step by step along the particle contour (see Figure 2). A similar concept was followed for pattern analysis in the past (Bennett and MacDonald, 1975; Persoon and Fu, 1977; Arkin et al., 1991). Recently in (Torgashov, 2014) motion vectors where represented as complex sequences and cross-correlated with templates for recognition purposes. Here, we are interested in morphological analysis. For this purpose, we examine the pixel motion along the boundary to sense relevant and distinctive characteristics of the particle contour, such as the succession and the curvature of curves, and the length of straight lines in order to perform efficient classification of dust particles shape.

These characteristics are extracted by looking at the collection of azimuth angles of the motion vectors, which measures the direction of the generic pixel during its step by step move along the contour. Let us assemble these angles φ_l in the new single column matrix Φ_k:

$$\Phi_k = \begin{bmatrix} \varphi_1 \\ \cdots \\ \varphi_l \\ \cdots \\ \varphi_L \end{bmatrix} , \tag{4}$$

being

$$\varphi_l = \arctan 2 \left(\delta_{yl}, \delta_{xl} \right) , |\varphi_l| < \pi , \tag{5}$$

where $\arctan 2 \left(\delta_y, \delta_x \right)$ is the four quadrant arctangent.

The incremental angles are then defined as

$$\Delta_{\varphi k} = \begin{bmatrix} \delta_{\varphi 1} \\ \cdots \\ \delta_{\varphi l} \\ \cdots \\ \delta_{\varphi L} \end{bmatrix} , \tag{6}$$

where

$$\delta_{\varphi l} = \varphi_{l \bmod L+1} - \varphi_{(l-1) \bmod L+1} . \tag{7}$$

The incremental angles $\delta_{\varphi l}$ are multiples of 45°, which is a very crude quantization. By fact, $\Delta_{\varphi k}$ represents the particle boundary at a very small scale. This is clearly visible in Figure 4 where the plot of the $\delta_{\varphi l}$ values calculated for the ideal particle of Figure 3 is displayed.

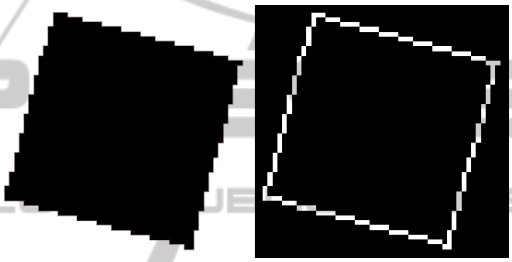

Figure 3: The shadow of an ideal particle (left) along with its boundary (right).

In order to obtain an interpretable plot, it is first necessary to attenuate the space quantization by smoothing the boundary.

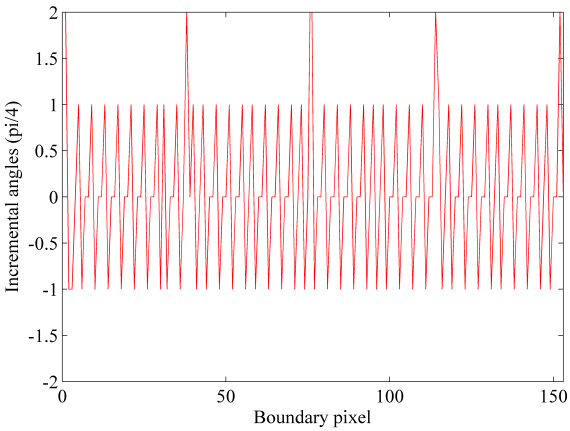

Figure 4: The incremental angle of the motion vector for each boundary position for the particle of Figure 3.

A very intuitive smoothing technique consists of measuring the matrix of angles after M moves:

$$\Phi_k^M = \begin{bmatrix} \varphi_1^M \\ \cdots \\ \varphi_l^M \\ \cdots \\ \varphi_L^M \end{bmatrix} , \tag{8}$$

being

$$\varphi_l^M = \arctan 2\left(\delta_{yl}^M, \delta_{xl}^M\right), \left|\varphi_l^M\right| < \pi, \tag{9}$$

and

$$\begin{aligned} \delta_{xl}^M &= \sum_{i=l}^{l+M-1} \delta_{x,i \bmod L}, \\ \delta_{yl}^M &= \sum_{i=l}^{l+M-1} \delta_{y,i \bmod L}. \end{aligned} \tag{10}$$

The incremental angles are assembled in the matrix:

$$\Delta_{\varphi k}^M = \begin{bmatrix} \delta_{\varphi 1}^M \\ \cdots \\ \delta_{\varphi l}^M \\ \cdots \\ \delta_{\varphi L}^M \end{bmatrix}, \tag{11}$$

where

$$\delta_{\varphi l}^M = \varphi_{l \bmod L+1}^M - \varphi_{(l-1) \bmod L+1}^M. \tag{12}$$

Phase unwrapping is performed by choosing at each point:

$$\hat{\delta}_{\varphi l}^M = \delta_{\varphi l}^M + 2\pi \underset{k\in\{-1,0,1\}}{\operatorname{argmin}} \left\{ \left| \delta_{\varphi l}^M + 2k\pi \right| \right\}. \tag{13}$$

The plot of these angles for the particle of Figure 3 after contour smoothing is shown in Figure 5.

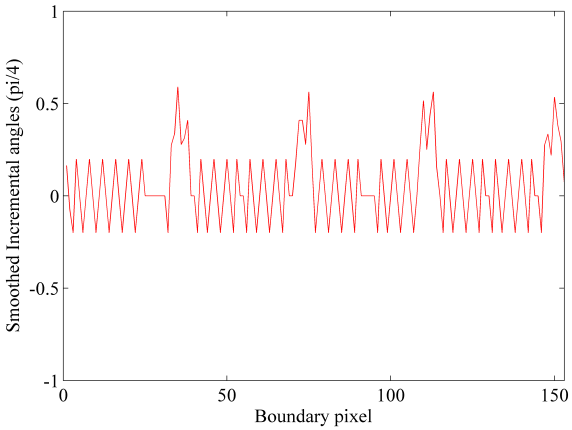

Figure 5: The incremental angle of the motion vector after smoothing of the contour of the particle of Figure 3, with M=6.

However, this sequence is still too noisy. A second filter is then applied to the sequence $\hat{\delta}_{\varphi l}^M$ in order to reject the residual angle quantization noise, yielding the filtered angle sequence assembled in the vector $\bar{\Delta}_{\varphi k}^N$:

$$\bar{\Delta}_{\varphi k}^N = \begin{bmatrix} \bar{\delta}_{\varphi 1}^N \\ \cdots \\ \bar{\delta}_{\varphi l}^N \\ \cdots \\ \bar{\delta}_{\varphi L}^N \end{bmatrix}, \tag{14}$$

where

$$\bar{\delta}_{\varphi l}^N = \frac{1}{N} \sum_{i=l-N+1}^{l} \delta_{\varphi \cdot (i \bmod L)}^M. \tag{15}$$

which is a circular moving average FIR filter. More elaborate filters could be devised, but in our experiments we have adopted this filter for simplicity.

The final result of this two stage angular quantization noise suppression is clearly visible in Figure 6 where the plot of the $\bar{\delta}_{\varphi l}^N$ values calculated for the same pattern of Figure 3 is shown. Now, the nature of the particle is revealed by long sequences of small incremental angles interrupted by peaks corresponding to abrupt vertices. This example reveals how much the sequence of incremental angles, (which is nothing else but the sequence of local curvature estimates) is suited for morphological analysis.

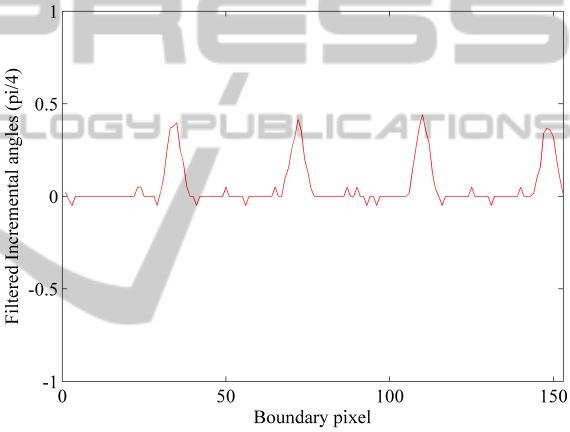

Figure 6: The incremental angle of the motion vector after smoothing and angle filtering for the particle of Figure 3, with M=6 and N=4.

In summary, the flowchart of the processing steps is reported in Figure 7. It terminates with the proposed particle classification algorithm, described in the next section.

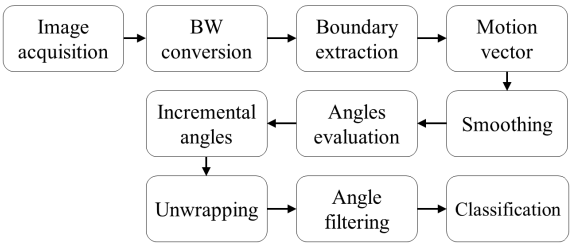

Figure 7: Flowchart of the proposed method.

4 PARTICLE CLASSIFICATION

In the present application, particle classification is based on measuring their dimension and on calculating a metric for distinguishing dust from fibre shapes.

An obvious indicator of the particle dimension is the length L of the $\bar{\delta}^N_{\varphi l}$ sequence. As far as the shape metric is concerned, let us preliminarily consider the typical shape of a $\bar{\delta}^N_{\varphi l}$ sequence for a dust particle, like the one shown in Figure 8.

Figure 8: The shadow of a typical dust particle (left) along with its boundary (right).

The shadow of these particles is characterized by a morphological compactness, which implies that the $\bar{\delta}^N_{\varphi l}$ sequence exhibits moderate oscillations around the average incremental steering of the boundary (see Figure 9). Of course, this average diminishes versus the particle size, while the sequence length grows.

By contrast, the shadows of fibres are characterized by long parallel contours with small curvature connected by abruptly steering terminations (see Figure 10). Thus, the typical shape of the $\bar{\delta}^N_{\varphi l}$ exhibits two low valued extended intervals interrupted by two peaks corresponding to terminations (see Figure 11).

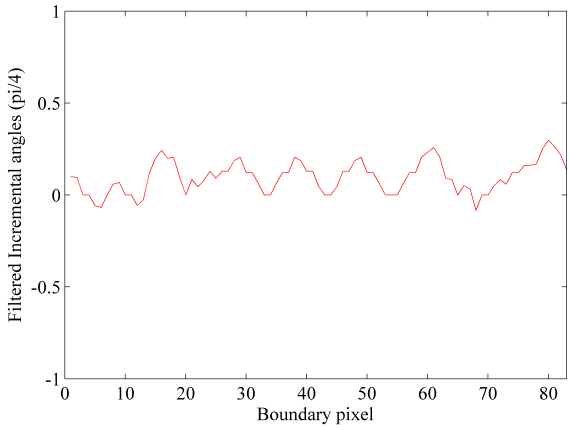

Figure 9: The incremental angle versus the boundary position for the dust particle of Figure 8 after smoothing and angle filtering, with M=6 and N=4.

Figure 10: The shadow of a typical fibre particle (left) along with its boundary (right).

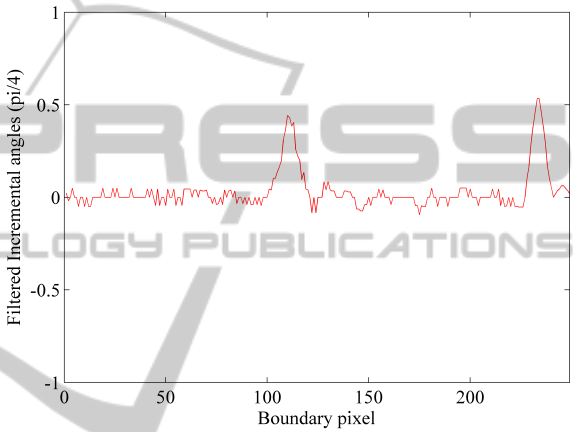

Figure 11: The incremental angle versus the boundary position for the fibre particle of Figure 10 after smoothing and angle filtering, with M=6 and N=4.

Such a different behaviour of the incremental angle is adequately captured by a metric constituted by the so called *varimax norm*, defined as follows:

$$V = L \frac{\Sigma_{l=1}^{L} \left[\bar{\delta}^N_{\varphi l} - \mu\right]^4}{\left\{\Sigma_{l=1}^{L} \left[\bar{\delta}^N_{\varphi l} - \mu\right]^2\right\}^2}, \tag{16}$$

where

$$\mu = \frac{1}{L} \sum_{l=1}^{L} \bar{\delta}^N_{\varphi l}. \tag{17}$$

In fact, interpreting $\bar{\delta}^N_{\varphi l}$ as samples of a random time series, the varimax norm is an estimate of its marginal kurtosis. Then, it may be inferred that V for dust particles should be close to 3 because their $\bar{\delta}^N_{\varphi l}$ sequences resemble realizations of Gaussian processes. Instead, it should assume much higher values for fibres, due to the presence of isolated peaks against a nearly Gaussian background (raising the tails of the marginal distribution).

This expected behaviour is confirmed by experiments. In Figure 12 examples of particles are shown

Figure 12: Some patterns from captured images.

along with associated V values described in Table 1. This simple behaviour allows using a threshold rule to discriminate dust against fibre particles. If V exceeds a threshold T, then the particle is classified as fibre.

Table 1: The varimax values respectively related to the sample patterns of Figure 12 (in the same order), with M=6 and N=4.

17.46	1.17	4.87	1.43	18.64	1.47	5.15	4.6

It is clear that fibre particles are characterized by high values of V, typically exceeding 10, while dust particles have V values typically less than three. Intermediate values of V correspond to rare particles that are hardly better discriminated without additional information, coming from instance from microscopic inspection.

Still, a first statistical assessment of the method was provisionally conducted using human classification as a reference for a set of particles drawn from available images (see Figure 13).

Figure 13: The test image used for automatic/manual classification comparison.

This set was used as a training set for selecting good parameters for automatic classification, yielding

$$M = 6\,, N = 4\,, T = 4\,. \tag{18}$$

Applying these parameters values to other test images, containing 250 objects not included in the training set and equally distributed among fibres and dust, the results shown by the confusion matrix in Table 2 were obtained.

The above classification differences are merely indicative, since reference data are subjective findings of human observers.

For comparison purpose, the classification experiment was repeated using the varimax norm and three well-known classifiers, i.e., the k-nearest neighbour classifier, the Naive Bayes classifier (Mitchell, 1997) and the Sugeno-type FIS (Chiu, 1994).

Table 2: The confusion matrix of the automatic versus manual labelling.

		Automatic classified shapes		
		Dust	Fibres	Matching (%)
Manual labelled shapes	Dust	119	6	95.2
	Fibres	3	112	97.6
Global matching				96.4

Table 3: Comparison of results performed with the other classifiers using the single varimax norm as feature.

Classifiers	k-nn	NaiveBayes	Sugeno FIS
Matching (%)	92.64	94.34	88.68

Results reported in Table 3 support the highly satisfactory classification performance of the proposed technique. Automated threshold selection technique did not exhibit any advantage compared to the selection of made on the above a priori considerations.

In order to further assess the goodness of the proposed method, a comparison was performed with a multi-features classification based on four shape features (length of the boundary, its surrounding area and the lengths of the principal axes of the equivalent elliptical contour), using the same three aforementioned classifiers. These tests, reported in Table 4, exhibit similar or worst performance with respect to the proposed approach, though implying higher computation cost.

Table 4: Comparison of results obtained with additional shape features.

Classifiers	k-nn	NaiveBayes	Sugeno FIS
Matching (%)	90.57	96.22	92.45

Future work will include statistical comparison with objective dust classification data obtained with laboratory equipment, in order to estimate the error rate of the method with high precision.

5 COMPUTATIONAL COST

After the image threshold operation, the classification of each particle entails the following computation steps:

- boundary tracking, which requires only logical operations.
- backward difference, requiring $2L$ additions.
- $2M \cdot L$ increments to determine motion vectors, and computation of their angles (conveniently done with a look-up table).
- circular moving average, which requires $N \cdot L$ additions.
- unwrapping, requiring $2L$ additions and magnitude comparisons.
- calculus of the mean value and the standard deviation of angles, requiring $2(L-1)$ sums and L squares.
- calculus of centred fourth order moments requiring $L-1$ sums and L fourth degree powers.

In substance, most of the computational cost is constituted by the $N \cdot L$ additions used for contour smoothing, and the final $2L$ powers.

These costs are small compared to the ones involved by classical feature based shape classification techniques, requiring multiple scale filters, Fourier transform, Radon transform, covariance, search of maxima, etc.

6 CONCLUSIONS

The steering angles of the contours are important indicators of the morphology of the particle shadows. They allow effective particle classification using mostly sum based processing. The advantages of the method herein presented are the simplicity of the imaging apparatus and the low computational cost of the classification process, which makes it especially suited for distributed sensing applications.

REFERENCES

Anderson, J., Thundiyil, J., and Stolbach, A. (2012). Clearing the air: A review of the effects of particulate matter air pollution on human health. *Journal of Medical Toxicology*, 8(2):166–175.

Arkin, E., Chew, L., Huttenlocher, D., Kedem, K., and Mitchell, J. (1991). An efficiently computable metric for comparing polygonal shapes. *Pattern Analysis and Machine Intelligence, IEEE Transactions on*, 13(3):209–216.

Bennett, J. R. and MacDonald, J. S. (1975). On the measurement of curvature in a quantized environment. *IEEE Transactions on Computers*, C-24(8):803–820.

Chichinadze, M. and Kvavadze, E. (2013). Pollen and non-pollen palynomorphs in organic residue from the hoard of ancient vani (western georgia). *Journal of Archaeological Science*, 40(5):2237 – 2253.

Chiu, S. L. (1994). Fuzzy model identification based on cluster estimation. *Journal of intelligent and Fuzzy systems*, 2(3):267–278.

Coronas, M., Bavaresco, J., Rocha, J., Geller, A., Caramo, E., Rodrigues, M., and Vargas, V. (2013). Attic dust assessment near a wood treatment plant: Past air pollution and potential exposure. *Ecotoxicology and Environmental Safety*, 95:153–160.

Delgado-Saborit, J., Stark, C., and Harrison, R. (2011). Carcinogenic potential, levels and sources of polycyclic aromatic hydrocarbon mixtures in indoor and outdoor environments and their implications for air quality standards. *Environment International*, 37(2):383–392.

Foi, A., Katkovnik, V., and Egiazarian, K. (2007). Pointwise shape-adaptive dct for high-quality denoising and deblocking of grayscale and color images. *IEEE Transactions on Image Processing*, 16(5):1395–1411.

Frontczak, M. and Wargocki, P. (2011). Literature survey on how different factors influence human comfort in indoor environments. *Building and Environment*, 46(4):922–937.

Jones, A. (1999). Indoor air quality and health. *Atmospheric Environment*, 33(28):4535–4564.

Kyropoulou, D. (2013). Scanning electron microscopy with energy dispersive x-ray spectroscopy: An analytical technique to examine the distribution of dust in books. *Journal of the Institute of Conservation*, 36(2):173–185.

Mitchell, T. M. (1997). *Machine Learning*. McGraw-Hill, Inc., New York, NY, USA, 1 edition.

Ozga, I., Bonazza, A., Ait Lyazidi, S., Haddad, M., BenNcer, A., Ghedini, N., and Sabbioni, C. (2013). Pollution impact on the ancient ramparts of the moroccan city sal. *Journal of Cultural Heritage*, 14(3 SUPPL):S25–S33.

Persoon, E. and Fu, K. (1977). Shape discrimination using fourier descriptors. *IEEE Transactions on Systems, Man and Cybernetics*, 7(3):170–179.

Proietti, A., Leccese, F., Caciotta, M., Morresi, F., Santamaria, U., and Malomo, C. (2014). A new dusts sensor for cultural heritage applications based on image processing. *Sensors (Switzerland)*, 14(6):9813–9832.

Torgashov, P. (2014). Contour analysis for image recognition in c#.